Railway Sciences

Cooperative traction control of multi-motor electric locomotives considering axle load transfer

Liran Li
AC Transmission Department,
China Academy of Railway Sciences Corporation Limited, Beijing, China
Simo Chen
Department of AC-Transmission Development,
China Academy of Railway Sciences Corporation Limited, Beijing, China
Kan Liu
China Academy of Railway Sciences Corporation Limited,
Locomotive and Car Research Institute, Beijing, China
Leiting Zhao
Department of AC Transmission,
China Academy of Railway Sciences Corporation Limited, Beijing, China, and
Xiaoming Liao
China Academy of Railway Sciences Corporation Limited, Beijing, China

Received 21 April 2026
Revised 20 May 2026
Accepted 26 May 2026

Abstract

Purpose – This study aims to propose a cooperative adhesion control method for multi-motor electric locomotives that explicitly considers axle load transfer (ALT). The method is intended to optimize the output torque of each motor, maximize the utilization of available wheel-rail adhesion within the total torque command, mitigate wheel skidding and sliding phenomena, and achieve optimal torque allocation across all axles.

Design/methodology/approach – An advanced cooperative maximum adhesion tracking control strategy is developed using Model Predictive Control (MPC). First, a comprehensive multi-agent dynamic model of the locomotive traction system is constructed based on Newton's second law, which incorporates longitudinal train dynamics, individual axle rotational dynamics, nonlinear wheel-rail adhesion characteristics, and dynamic ALT-induced load redistribution. Then, a novel MPC-based multi-axle co-optimization method is presented. This controller calculates the optimal output torque through real-time iteration based on a reference slip speed, ensuring coordinated torque allocation under strict physical constraints imposed by the traction control unit.

Findings – Simulation studies conducted under dry, wet, and mixed rail surface conditions indicate that the proposed MPC system effectively compensates for ALT. The results demonstrate that explicitly embedding ALT into the control framework allows the system to adaptively redistribute motor torques according to real-time axle loads. This guarantees stable slip regulation and significantly improves overall traction performance and power distribution compared to conventional strategies that ignore ALT.

Originality/value – This study introduces a novel cooperative adhesion tracking control scheme that uniquely integrates axle load transfer into a multi-agent MPC for multi-motor electric locomotives – a complex configuration rarely addressed in previous papers. This approach resolves the critical issues of torque imbalance,

Funding: This research is supported by the Fund of China Academy of Railway Sciences Corporation Limited (2025YJ055).

Railway Sciences
Emerald Publishing Limited
e-ISSN: 2755-0915
p-ISSN: 2755-0907
DOI 10.1108/RS-04-2026-0031

lightly loaded axle slip, and heavily loaded axle under-utilization, offering significant theoretical and practical value, especially under variable and non-uniform rail conditions.

Keywords Cooperative control, Multi-motor electric locomotive, Axle load transfer, Model predictive control
Paper type Research article

1. Introduction

The electrification of transportation has been steadily advancing and is becoming increasingly important in the railway sector (Georgatzi, Stamboulis, & Vetsikas, 2020). Compared with conventional locomotives, electric locomotives offer significant advantages in terms of energy efficiency and environmental impact. For reasons related to safety, performance, reliability, and energy economy, optimizing traction utilization has become a critical requirement in modern railway traction systems (Abouzeid *et al.*, 2024a). Achieving maximum adhesion utilization enables more efficient acceleration, reduces travel delays, and minimizes unnecessary energy consumption (Liu, Chen, & Wang, 2023). Therefore, a control method capable of maximizing available traction is essential to the development of advanced train traction systems.

The magnitude of a train's traction force depends not only on the output torque of the traction motors but also on the wheel-rail adhesion coefficient. The adhesion coefficient varies continuously due to factors such as oil contamination, fallen leaves, ice, and snow on the rail surface. When the traction or braking torque applied by the motors exceeds the available adhesion, wheel slip or wheel slide occurs. In extreme cases, excessive slip may even lead to derailment or other hazardous incidents.

To prevent excessive wheel slip and ensure operational safety, a wide range of anti-slip and re-adhesion control strategies have been developed. Kadowaki *et al.* (2007) developed a re-adhesion control method that combines sensorless vector control with a disturbance observer, which was applied to the JR East Series 205-5000 trains to improve adhesion recovery performance. Spiryagin, Lee, and Yoo (2008) presented a traction control system that integrates an observer with a fuzzy controller, where the wheel–rail friction conditions (including slip ratio, load, and lateral displacement) are estimated in real time, and the adhesion coefficient is indirectly identified through noise spectrum analysis. Yamashita and Soeda (2015) proposed an anti-slip re-adhesion control method that enhances tractive force by detecting wheel slip convergence early using acceleration signals with reduced delay, which was validated through simulations and running tests on an HD300-type shunting locomotive. Uyulan and Gokasan (2018) presented a re-adhesion control method based on a modified super-twisting sliding mode algorithm for an induction motor-based railway traction system. Wen, Huang, and Zhang (2019) proposed a distributed MPC-based anti-slip re-adhesion control strategy for electric locomotives to suppress wheel slip by constraining the adhesion zone and incorporating slack variables. Although these re-adhesion control approaches are effective in mitigating wheel slip and improving operational safety, they are generally conservative in nature and do not explicitly maximize adhesion.

It is well established that the wheel-rail adhesion coefficient exhibits strong nonlinearity (Ishikawa & Kawamura, 1997; Yuan, Wu, Tian, Zhou, & Chen, 2021) with respect to creep velocity and is subject to significant uncertainties, which has motivated the adoption of advanced control and predictive control (Sadr, Khaburi, & Rodríguez, 2016) approaches. Chen, Dong, Lu, Sun, and Guo (2016) developed a train operation control strategy that achieves near-optimal utilization of wheel-rail adhesion by employing a super-twisting-like algorithm to enhance robustness against adhesion uncertainties. Moaveni, Fathabadi, and Molavi (2020) proposed a supervisory model predictive control (MPC) system for electric trains that uses field-oriented control to regulate wheel angular speed and a fuzzy supervisor to coordinate train longitudinal velocity and slip, with real-time estimation of adhesion coefficient to ensure effective adhesion control. Diao, Zhao, Jin, Wang, and Sharkh (2017) introduced a high-adhesion-point tracking traction control method using a first-order disturbance observer

combined with a dynamic torque tuning function to enhance adhesion efficiency and robustness under varying rail conditions. Abouzeid *et al.* (2024b) investigated two advanced maximum adhesion tracking strategies based on fuzzy logic control and particle swarm optimization, which were validated through simulations and experiments on a scaled roller rig, showing improved search speed, reduced torque ripple, and enhanced adhesion utilization compared to conventional methods. Although these works have advanced adhesion and slip-prevention control, they do not explicitly account for ALT and its influence on per-axle adhesion capacity.

During traction and braking phases, ALT inevitably alters the normal forces acting on individual wheelsets, thereby changing their available adhesion forces, which are directly proportional to the axle loads. Neglecting axle-load transfer can lead to significant torque imbalance among axles, reduced adhesion utilization, increased risk of wheel slip on lightly loaded axles and under-utilization on heavily loaded axles, degraded acceleration/braking performance (Liu, Jiang, Zhao, Wen, & Jin, 2020). In extreme cases, this can compromise structural integrity (Ma *et al.*, 2025) and jeopardize operational safety. Hence, incorporating ALT into adhesion and traction control is essential for both performance and safety. Chen, Ge, Chen, Wang, and Wang (2025) proposed a nonlinear optimisation method to allocate traction forces among locomotive axles in a way that improves adhesion utilisation, while explicitly accounting for axle-load transfer caused by an oblique traction rod. Guo and He (2024) developed a dynamic optimal allocation strategy for electric and pneumatic braking forces that considers axle load transfer. By estimating the adhesion capacity of each wheelset in real time and formulating a linear programming model to maximize adhesion utilization, the method adaptively distributes braking forces and thereby enhances the braking stability and safety of high-speed trains. Liu, Wu, Ma, and Yuan (2025) proposed a model-driven framework that integrates ALT-aware traction optimization with an Unscented Kalman Filter-based adhesion estimation strategy, demonstrating its effectiveness in resolving gradient-starting traction limitations of heavy-haul locomotives, where representative gradient-starting failure cases were reported and analyzed.

This paper proposes a multi-motor cooperative traction control framework based on MPC that explicitly accounts for axle load transfer, with the objective of maximizing available tractive force and preventing traction insufficiency under varying adhesion conditions. The rest of this paper is structured as follows. First, a comprehensive multi-agent dynamic model of the locomotive is developed, incorporating the vehicle longitudinal dynamics, axle load transfer mechanism, and nonlinear wheel–rail adhesion characteristics. Then, an MPC-based cooperative controller is designed to achieve optimal adhesion utilization by dynamically coordinating the torque outputs of multiple traction motors under varying rail surface conditions. Finally, simulation studies are conducted under several operating scenarios, including dry and wet rail surfaces, as well as mixed surface conditions.

2. System modeling of a multi-motor locomotive with ALT

2.1 Wheel–rail adhesion and creep characteristics

For a four-axle electric locomotive, a creep phenomenon occurs at the wheel–rail interface during operation due to the elastic deformation and compression between the wheel and the rail. The creep characteristics are commonly described by the wheel–rail adhesion coefficient. The adhesion coefficient μ is a stochastic variable and exhibits a nonlinear relationship with the creep velocity (Huang *et al.*, 2021). For the i-th wheelset, the creep velocity v_s^i is defined as the difference between the wheel circumferential speed v_w^i and the train running speed v_t:

$$v_s^i = v_w^i - v_t. \tag{1}$$

μ^{i} is highly correlated with the rail surface and wheel conditions. The empirical formula for calculating the adhesion characteristic curve is given by Lu, Song, and Cai (2014), Molavi and Rashidi Fathabadi (2022), Zhao *et al.* (2019)

$$\mu^i\left(v_s^i\right) = ce^{-av_s^i} - de^{-bv_s^i}. \tag{2}$$

where the parameters *a*, *b*, *c* and *d* are related to the rail surface condition. The parameter values under two types of rail surfaces are shown in Table 1, and Figure 1 shows the corresponding adhesion characteristic curves as functions of the creep velocity. It can be seen that the empirical formula parameters differ depending on the rail surface condition. In practical onboard applications, such adhesion-related parameters are not directly measurable and are typically inferred from available dynamic measurements using dedicated sensors or observer-based estimation schemes. In this study, it is assumed that the required adhesion information can be provided to the controller by such existing estimation modules, and the problem of real-time adhesion estimation itself is beyond the scope of this paper. In practical onboard applications, such adhesion-related parameters are not directly measurable and are typically inferred from available dynamic measurements using observer-based estimation schemes, see, e.g. (Can, Jingchun, Wenqi, & Xiaokang, 2019; Moaveni *et al.*, 2020). In this study, it is assumed that the required adhesion information can be provided to the controller by existing estimation modules, and the problem of real-time adhesion estimation is beyond the scope of this paper.

As the only driving force that propels the locomotive forward, the adhesion force F_s^i of the *i*-th wheelset can be expressed as

$$F_s^i = \mu^i\left(v_s^i\right)W^i, \tag{3}$$

Table 1. Parameter values under two types of rail surfaces

Rail surface condition	a	b	c	d
Dry	0.54	1.2	1.0	1.0
Wet	0.19	0.54	0.4	0.4

Source(s): Authors' own work

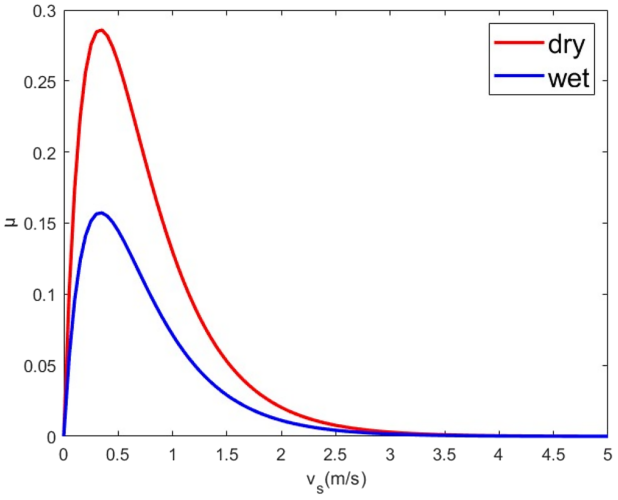

Figure 1. Adhesion characteristic curve. Source: Authors' own work

where $\mu^i(v_s^i)$ denotes the wheel-rail adhesion coefficient as a function of the creep velocity v_s^i, W^i is the vertical load on the *i*-th wheelset, and *g* is the gravitational acceleration.

2.2 Axle load transfer

In dynamic modeling, the axle loads are commonly assumed to be uniformly distributed. However, when the locomotive develops traction, the vertical reaction forces and the center of gravity do not lie on the same line of action. Combined with the effects of train structure, track conditions, and running speed, the center of gravity shifts, resulting in a redistribution of axle loads, which is referred to as axle load transfer. If the traction torques of the four traction motors are not appropriately adjusted, the variation in axle load may lead to wheel slip on lightly loaded axles and insufficient traction on heavily loaded axles.

To analyze the axle load transfer during the starting and acceleration process, a B_0-B_0 type four-axle electric locomotive is considered. As shown in Figure 2, the axles are numbered from 1 to 4 along the forward running direction of the locomotive, and a force analysis is performed for each axle.

Let the total axle load of the locomotive be denoted by *W*,

$$W = Mg, \tag{4}$$

where *M* is the total mass of the locomotive. And the axle loads of the four wheelsets are denoted by W^1, W^2, W^3 and W^4, respectively. The vertical force equilibrium of the locomotive is given by

$$W^1 + W^2 + W^3 + W^4 = W. \tag{5}$$

When the locomotive is stationary or no longitudinal acceleration is present, the axle loads are evenly distributed, i.e.,

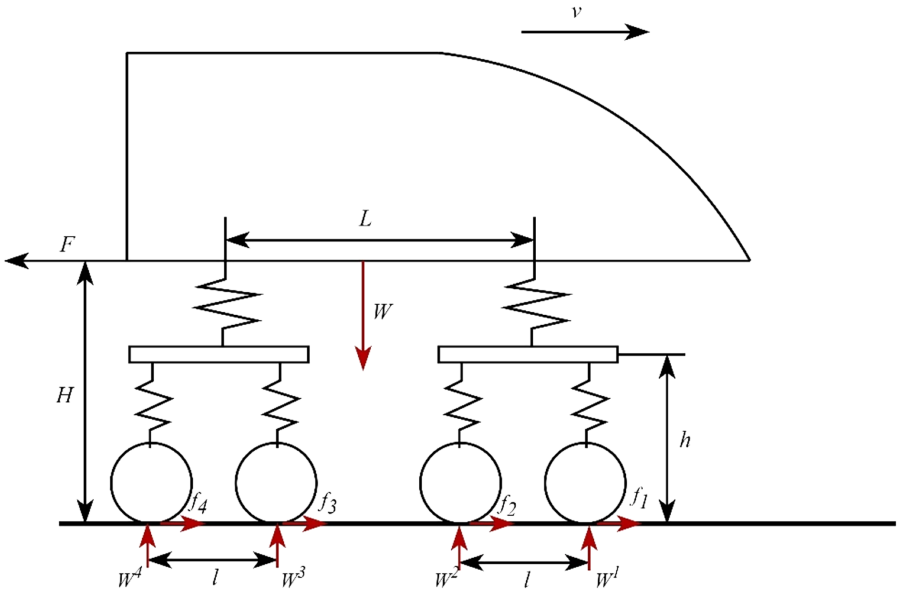

Figure 2. Locomotive with four wheelsets and force analysis. Source: Authors' own work

$$W^1 = W^2 = W^3 = W^4 = \frac{W}{4}. \tag{6}$$

During locomotive operation, the total traction force is equal to the total adhesion force, that is

$$F = \sum_{i=1}^{4} F_s^i \tag{7}$$

$$F_s^i = f_i, \tag{8}$$

where f_i represents the static friction force on the i-th wheelset. The actual axle loads during operation can be expressed accordingly (Moaveni *et al.*, 2020):

$$\begin{cases} W^1 = \dfrac{W}{4} - \dfrac{H-h}{2L}F - \dfrac{h}{l}(f_1 + f_2) \\ W^2 = \dfrac{W}{4} - \dfrac{H-h}{2L}F + \dfrac{h}{l}(f_1 + f_2) \\ W^3 = \dfrac{W}{4} + \dfrac{H-h}{2L}F - \dfrac{h}{l}(f_3 + f_4) \\ W^4 = \dfrac{W}{4} + \dfrac{H-h}{2L}F + \dfrac{h}{l}(f_3 + f_4) \end{cases} \tag{9}$$

Here the symbols are:

(1) H: height from rail to coupler,

(2) h: height from rail to the bogie traction point,

(3) I: axle spacing within a bogie,

(4) L: distance between bogie centers.

2.3 Multi-agent locomotive dynamic model with axle load transfer

With the actual axle loads obtained considering the axle load transfer, the overall longitudinal dynamics of the locomotive can be formulated as:

$$M\frac{dv_t}{dt} = \sum_{i=1}^{n} F_s^i - F_d, \tag{10}$$

where the running resistance F_d is modeled as

$$F_d = \alpha + \beta v_t + \gamma v_t^2, \tag{11}$$

with v_t denoting the train speed, F_s^i the adhesion force, and α, β, γ being the Davis resistance coefficients.

The rotational dynamics of the traction motor on the i-th axle are given by

$$J_m^i \frac{d\omega_m^i}{dt} = T_m^i - T_L^i, \tag{12}$$

where ω_m^i denotes the motor angular speed, T_m^i is the motor output torque, J_m^i is the rotational inertia of the motor, and T_L^i is the load torque reflected to the motor shaft due to wheel-rail adhesion.

The rotational dynamics of the wheelset on the *i*-th axle are described as

$$J_d^i \frac{d\omega_d^i}{dt} = T^i - F_s^i r, \tag{13}$$

where ω_d^i is the angular speed of the wheelset, $T^i = R_g T_L^i$ is the transmitted torque through the gearbox, $R_g = \frac{\omega_m^i}{\omega_d^i}$ is the gear ratio, J_d^i is the rotational inertia of the wheelset, and r is the wheel radius.

Combining the above motor-wheelset dynamics yields the equivalent rotational dynamic model referred to the motor shaft:

$$J_{eq}^i \frac{d\omega_m^i}{dt} = T_m^i - \frac{r}{R_g}\mu^i\left(v_s^i\right)W^i, \tag{14}$$

where the equivalent inertia is

$$J_{eq}^i = J_m^i + \frac{J_d^i}{R_g^2}. \tag{15}$$

The traction system dynamic model of a multi-motor locomotive is formulated as follows:

$$\begin{cases} \dfrac{dv_s^i}{dt} = \dfrac{r}{R_g J_{eq}^i}T_m^i - \dfrac{r^2 W^i}{R_g^2 J_{eq}^i}\mu^i\left(v_s^i\right) - \dfrac{1}{M}\displaystyle\sum_{j=1}^{n} W^j \mu^j\left(v_s^j\right) + \dfrac{\alpha + \beta v_t + \gamma v_t^2}{M}, \\ \dfrac{dv_t}{dt} = \dfrac{1}{M}\displaystyle\sum_{j=1}^{n} W^j \mu^j\left(v_s^j\right) - \dfrac{\alpha + \beta v_t + \gamma v_t^2}{M}. \end{cases} \tag{16}$$

The model (16) is a multi-input multi-output system, in which each axle–motor unit possesses its own states, control inputs, and outputs. Owing to this structure and the dynamic coupling among axle units through the longitudinal motion of the locomotive, the overall system can be naturally regarded as a multi-agent system, where each axle–motor unit is regarded as an agent.

3. Cooperative controller design

In this section, we use a model predictive control approach, based on the previously discussed multi-agent model, to jointly optimize the output torque of each motor in the multi-motor locomotive system.

3.1 System discretization

Let $v_s^{ref} = [v_s^{1,ref}, v_s^{2,ref}, ..., v_s^{n,ref}]^T$, to achieve the tracking of the reference slip speed $v_s^{i,ref}$ for any i-axle, the objective function of the predictive controller at time step k is formulated as follows:

Define the state vector as $x = [v_s^1, v_s^2, \ldots, v_s^n, v_t]^T$, the control input vector as $u = [T_m^1, T_m^2, \ldots, T_m^n]^T$, and the output vector as $y = [v_s^1, v_s^2, \ldots, v_s^n]^T$. The state space equation (16) of the system can be expressed as:

$$\dot{x} = f(x,u), \tag{17}$$

$$y = Cx, \tag{18}$$

where $C = [I_{n*n}\ 0]$. The system is a dynamically coupled nonlinear multi-agent system with n inputs and n outputs.

To facilitate the controller design, the state space equation is first discretized to obtain the offline model as:

$$x(k+1) = x(k) + Tf(x(k),u(k)) = F(x(k),u(k)) \tag{19}$$

where T is the periodic sampling time interval. To be more explicit, the discrete-time system dynamic is given by

$$\begin{cases} v_s^i(k+1) = v_s^i(k) + T\left(\begin{array}{c} \dfrac{r}{R_g J_{eq}^i} T_m^i(k) - \dfrac{r^2 W^i}{R_g^2 J_{eq}^i} \mu^i\left(v_s^i(k)\right) \\ -\dfrac{1}{M}\displaystyle\sum_{j=1}^{n} W^j \mu^j\left(v_s^j(k)\right) + \dfrac{\left(\alpha + \beta v_t(k) + \gamma v_t^2(k)\right)}{M} \end{array} \right) \\ v_t(k+1) = v_t(k) + T\left(\dfrac{1}{M}\displaystyle\sum_{j=1}^{n} W^j \mu^j\left(v_s^j(k)\right) - \dfrac{\alpha + \beta v_t(k) + \gamma v_t^2(k)}{M} \right) \end{cases} \tag{20}$$

3.2 MPC controller

MPC determines the optimal control actions by minimizing a performance-based objective function. This objective function is formulated according to the system control requirements, while operational constraints on the control inputs and state variables are imposed based on train operation specifications. By solving this constrained optimization problem at each prediction step, MPC generates the optimal control sequence to achieve the desired dynamic performance.

To maximize the adhesion utilization under varying rail surface conditions, the objective function is defined as:

$$J(k) = \sum_{j=1}^{N_p} \left\| y(k+j|\,k) - v_s^{ref}(k+j|\,k) \right\|_Q^2 + \sum_{j=0}^{N_c-1} \left\| u(k+j|\,k) \right\|_R^2 \tag{21}$$

where:

(1) $J(k)$: objective function value at prediction step k,

(2) N_p: prediction horizon,

(3) N_c: control horizon,

(4) $y(k+j|\,k)$: the predicted system output, i.e. the vector of wheel slip velocities, at time step $k+j$ based on the information available at k,

(5) $v_s^{ref}(k+j|\,k)$: the reference slip velocity trajectory, which is provided by the traction control unit (TCU) based on existing adhesion management logic,

(6) $u(k+j|\,k)$: predicted control input sequence, and its absolute torque command,

(7) Q and R: positive definite weighting matrices that penalize adhesion deviation and control effort, respectively. Practically, we usually set Q much larger than R, since tracking the reference slip velocity trajectory is the main objective.

In addition, the system constraints are formulated as follows. Due to the physical limitations of the traction motors, the motor torque command of each axle is bounded by the maximum allowable torque imposed by the TCU, denoted by T_{lim}. Moreover, to satisfy the total traction capability constraint, the sum of the torques generated by all traction motors must not exceed the maximum admissible total torque, denoted by T_m^*. Accordingly, the input constraints can be expressed as

$$\begin{cases} T_m^i\,(k+j|\,k) \le T_{\lim}, i = 1,2,\ldots,n, \\ \sum_{i=1}^{n} \left(T_m^i(k+j|\,k)\right) \le T_m^*. \end{cases} \tag{22}$$

Based on the above objective function and system dynamic model as well as system constraints, the MPC optimization problem at time step k can be formulated as follows:

$$\min_{u(k+j|k)_{j=0}^{N_c-1}} J(k)$$

$$\text{s.t. } x(k|k) = x(k),$$

$$x(k+j+1|k) = F(x(k+j|k), u(k+j|k)), j = 0,1,\ldots,N_c-1$$

$$x(k+j+1|k) = F(x(k+j|k), u(k+Nc-1|k)), j = Nc,\ldots,Np-1$$

$$y(k+j|k) = Cx(k+j|k), j = 1,\ldots,N_p$$

$$T_m^i(k+j|\,k) \le T_{lim}, i = 1,2,\ldots,n, j = 0,\ldots,N_c-1$$

$$\sum_{i=1}^{n} T_m^i(k+j|\,k) \le T_m^*, j = 0,\ldots,N_c-1.$$

At each sampling instant k, the current system state x(k) is used as the initial condition. Based on the nonlinear discrete-time model (20), the system evolution over the prediction horizon N_p is predicted using the control input sequence $\{u(k|k), u(k+1|k), \ldots, u(k+N_c-1|k)\}$. A constrained nonlinear optimization problem is solved to obtain the optimal control sequence $\{u^*(k|k), u^*(k+1|k), \ldots, u^*(k+N_c-1|k)\}$, which minimizes the objective function subject to the system dynamics and constraints. According to the receding horizon principle, only the first control action $u^*(k|k)$ is applied to the system, and the optimization procedure is repeated at the next sampling instant.

4. Simulation and discussion

In this study, the multi-motor locomotive dynamic model described above is implemented in the MATLAB simulation environment to verify the effectiveness of the proposed model and control strategy. The train motor torque command limit is applied as the system constraint. At each sampling instant, the nonlinear MPC optimization problem is solved numerically using the built-in fmincon solver in MATLAB. Since a general nonlinear programming solver is adopted, the original nonlinear system model is used directly in the prediction stage, and no

linearization or model approximation is performed. The simulations focus exclusively on the acceleration phase, during which traction performance and adhesion utilization are most critical, while steady-speed cruising and braking phases are not considered in this study. The total simulation duration is set to 30*s*, and two different track surface conditions are considered: a dry track surface and a wet track surface. The values of related parameters are given explicitly in Table 2.

In the first case, the train starts on a dry track surface. At $t = 10s$, all four axles enter a wet track surface, and at $t = 20s$, they return to a dry track surface. The simulation results are shown in Figure 3.

Figure 3 presents the simulation results of the four-axle locomotive, where the reference slip velocity given by the TCU is set to $v_s^{ref} = 0.35\,m/s$. The maximum torque of each traction motor is limited to 5000Nm, and the total traction torque commanded by the TCU is constrained to 16500Nm. Under dry rail conditions, the controller operates under the total torque constraint imposed by the TCU. Consequently, the slip velocities cannot physically reach the unconstrained reference of 0.35m/s (indicated by the dashed lines in Figure 3(a). However, the system states remain strictly bounded and converge to a stable equilibrium.

The actual slip velocities of the four axles stabilize within the range of $0.230 - 0.234$m/s, while the corresponding adhesion coefficients are maintained at approximately 0.27. As shown in Figure 3(c) and (d), axle load transfer occurs during the acceleration phase. Specifically, Axles 1 and 3 experience load reduction, with the axle load of Axle 1 decreasing from 34709N to 31902*N*, and that of Axle 3 decreasing to 34302N. The corresponding motor torques of Axles 1 and 3 are 3883Nm and 4087Nm, respectively. In contrast, Axles 2 and 4 gain additional load, with the axle loads increasing to 35116*N* and 37515*N*, and the corresponding motor torques reaching 4171*Nm* and 4357*Nm*. When the track surface switches to wet conditions, the proposed MPC-based cooperative traction controller demonstrates excellent tracking performance and convergence properties. The motor torques are regulated such that the slip velocities of all axles rapidly converge to and stably track the reference value of 0.35m/s, as illustrated in Figure 3. Simultaneously, the adhesion coefficients of all axles converge to approximately 0.157, as shown in Figure 3(b). Although the magnitude of axle load transfer is alleviated under wet conditions, it remains non-negligible. The actual axle loads of Axles 1 to 4 are 33074N, 34946N, 34472N, and 36343N, respectively. Accordingly, the optimized motor torque outputs are adjusted to 2313Nm, 2424Nm, 2386Nm, and 2484Nm for Axles 1 to 4. These results demonstrate that the proposed control strategy effectively coordinates multi-motor torque outputs by accounting for axle load transfer, enabling stable slip regulation and improved traction utilization under both dry and wet rail surface conditions.

Next, a non-uniform adhesion scenario is investigated to evaluate the cooperative control capability and stability under heterogeneous wheel-rail conditions. The train initially operates on a dry track surface. At t = 10s, Axles 3 and 4 are assumed to experience a reduced adhesion condition equivalent to a wet surface, while Axles 1 and 2 remain on the dry surface. At t = 20s, all four axles return to dry conditions. It should be emphasized that this scenario is not intended to replicate a specific track geometry, but rather to represent a typical situation with

Table 2. Simulation parameter settings

Parameter	Value
Locomotive mass: M	14,167 kg
Gravitational acceleration: g	9.8 m/s^2
Wheel radius: r	0.5 m
Gear ratio: R_g	4.13
Equivalent rotational inertia: J_{eq}^i	146.7 $kg \cdot m^2$
Sampling time: T	0.1 s

Source(s): Table courtesy of Molavi and Rashidi Fathabadi (2022)

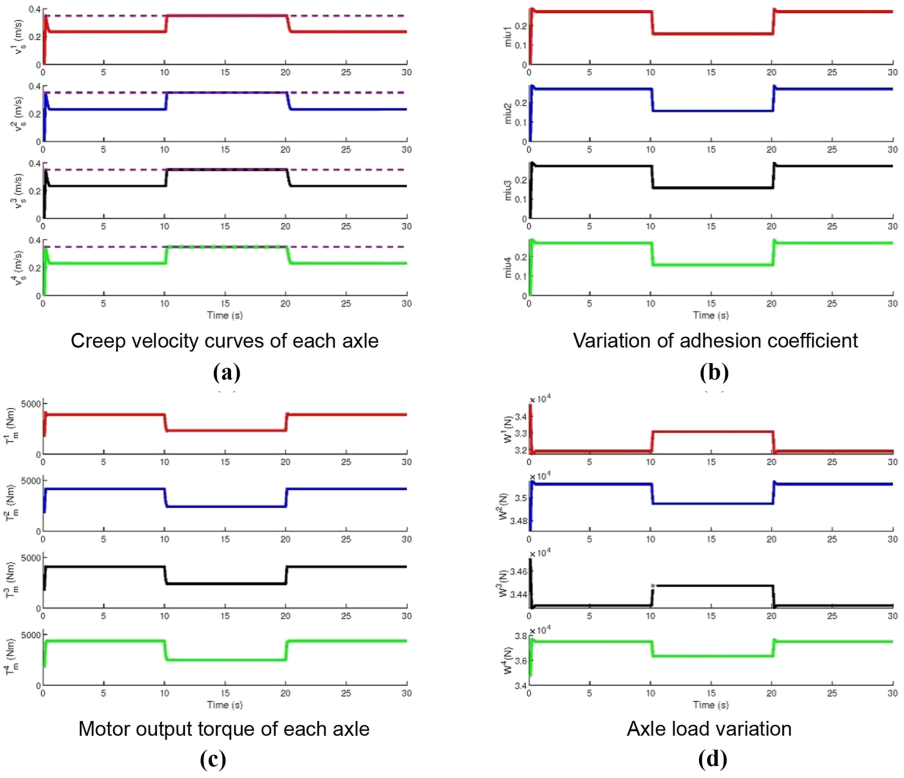

Figure 3. Simulation results of Case 1: alternating dry and wet rail surface conditions. Source: Authors' own work

non-uniform effective adhesion distribution among axles, which may arise due to localized rail contamination, wheel-rail contact variability, or environmental effects. Compared with the case where all axles experience identical adhesion variations, such heterogeneous conditions lead to more pronounced axle load redistribution and torque allocation conflicts, thereby posing a more challenging control problem regarding system stability. The simulation results are shown in Figure 4. Figure 4(a) presents the creep velocity responses of the four axles with respect to the reference creep velocity specified by the traction control unit (TCU), while Figure 4(b) illustrates the corresponding adhesion coefficient variations. The motor torque outputs and axle load transfers are depicted in Figure 4(c) and (d). The results indicate that despite the sudden change in adhesion conditions, the system maintains robust stability without significant oscillation. During the interval $10s < t < 20s$, Axle 1 experiences a noticeable load reduction to 32023N, whereas Axles 2-4 exhibit load increases of varying magnitudes, reaching 35426N, 34757N, and 36629N. Among them, Axle 4 shows the largest load increase, while Axle 3 experiences the smallest change. Correspondingly, the controller reallocates the motor torques to 3799Nm, 4123Nm, 2702Nm, and 2803Nm for Axles 1-4, respectively. These results demonstrate that the proposed MPC-based cooperative control strategy can effectively coordinate torque distribution among axles under heterogeneous adhesion conditions, while explicitly accounting for axle load transfer effects and maintaining operation near the reference creep velocity.

Finally, the simulation results of the system without considering axle load transfer are compared to reveal the potential risks caused by neglecting axle load transfer. When

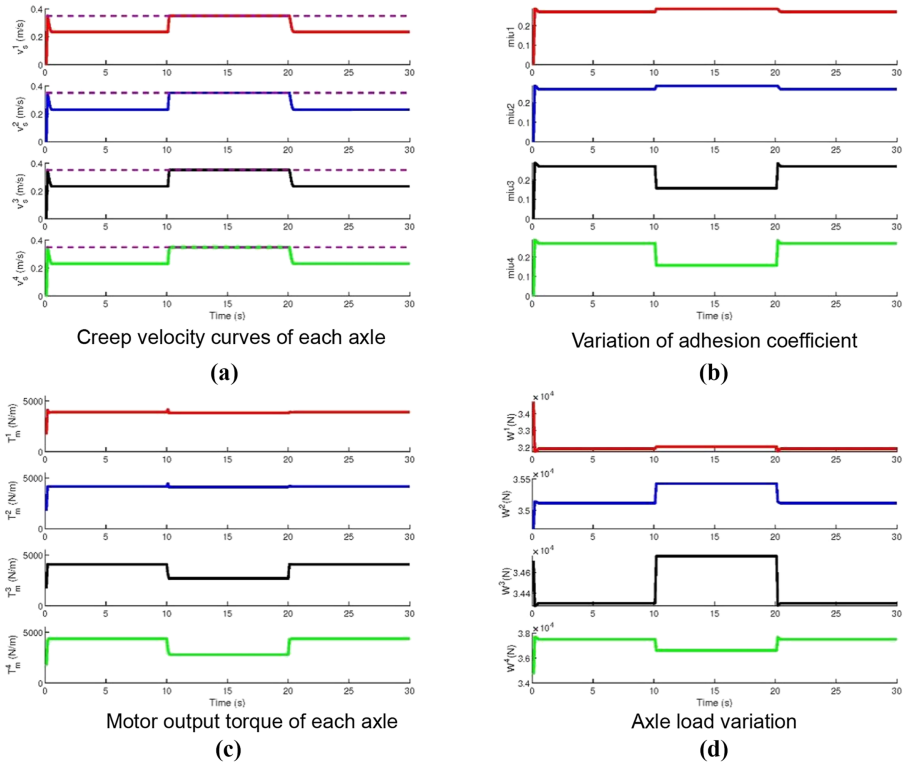

Figure 4. Simulation results of Case 2: alternating dry and wet rail surface conditions. Source: Authors' own work

neglecting axle load transfer, the axle loads are evenly distributed as shown in Eq. (6). Table 3 (Case 3) presents the motor output torques of each axle under dry rail surface conditions and identical traction demand. By comparing the output torques of each axle, it can be observed that under dry surface conditions, the maximum difference in motor output torque between Case 1 (considering ALT) and Case 3 (without ALT) reaches up to 5.5%. According to the adhesion characteristic curve as shown in Figure 1, when the adhesion coefficient reaches its peak value, any further increase in creep velocity (corresponding to increased torque) will cause wheel slip or even lead to traction loss and operational instability, which is more likely to occur in the case without considering axle load transfer. Therefore, adhesion control considering axle load transfer ensures safer operation and achieves better adhesion utilization compared to the case without axle load transfer.

Table 3. Comparison of motor output torques in Case 1 and Case 3

Dry	T_m^1	T_m^1	T_m^1	T_m^1
Case1 considering ALT	3881 *Nm*	4174 *Nm*	4086 *Nm*	4359 *Nm*
Case3 without ALT	4109 *Nm*	4141 *Nm*	4119 *Nm*	4131 *Nm*

Source(s): Table courtesy of Moaveni *et al.* (2020)

5. Conclusion

This paper establishes a multi-agent dynamic model for a multi-motor electric locomotive that explicitly accounts for ALT and nonlinear wheel–rail adhesion. By framing the system through a multi-agent lens, each traction motor operates as an individual agent with its own dynamic state, while the locomotive's overall motion is governed by their cooperative interaction via the shared train speed. This architecture allows the proposed MPC strategy to optimally coordinate torque allocation across multiple axles while strictly adhering to the physical constraints of the traction control unit. Simulation studies of the acceleration phase, conducted under both uniform and heterogeneous rail surface conditions, reveal that ALT significantly impacts achievable slip velocity and traction torque distribution. Crucially, even with sufficient available adhesion, uncompensated ALT and torque limits can degrade traction performance and cause conflicting torque demands among axles. By seamlessly integrating ALT dynamics into the MPC framework, the proposed strategy adaptively redistributes motor torques in real time, guaranteeing stable slip regulation and maximizing overall adhesion utilization.

Despite the promising simulation results, several limitations of this study should be acknowledged. First, the proposed control strategy is implemented as a centralized MPC, which requires global system information and solves a single optimization problem for all axle-motor units. While this centralized formulation enables coordinated traction optimization, it may face scalability and computational limitations as the system size increases. Moreover, the proposed controller has been validated primarily through numerical simulations. Although these simulations capture key traction and adhesion characteristics, direct experimental validation using real vehicles has not yet been conducted. In addition, uncertainties related to parameter variations, sensor noise, and actuator dynamics are not fully considered in the current model. Our future work will focus on further validating the proposed control strategy through semi-physical simulation and hardware-in-the-loop testing under more realistic operating conditions. In parallel, distributed and cooperative control architectures, such as distributed MPC frameworks, will be investigated to improve scalability, robustness, and real-time applicability for large-scale multi-motor locomotive systems. Ultimately, on-track experimental testing will be considered to evaluate the real-world applicability of the proposed approach.

References

Abouzeid, A. F., Guerrero, J. M., Lejarza-Lasuen, L., Muniategui-Aspiazu, I., Endemaño-Isasi, A., & Briz, F. (2024a). Advanced maximum adhesion tracking strategies in railway traction drives. *IEEE Transactions on Transportation Electrification*, *10*(2), 3645–3660. doi: 10.1109/TTE.2023.3312621.

Abouzeid, A. F., Guerrero, J. M., Lejarza-Lasuen, L., Muniategui-Aspiazu, I., Endemaño-Isasi, A., & Briz, F. (2024b). Advanced maximum adhesion tracking strategies in railway traction drives. *IEEE Transactions on Transportation Electrification*, *10*(2), 3645–3660. doi: 10.1109/TTE.2023.3312621.

Can, K., Jingchun, H., Wenqi, D., & Xiaokang, W. (2019). Adhesion control method based on optimal slip velocity searching and tracking. In *2019 14th IEEE International Conference on Electronic Measurement & Instruments (ICEMI)* (pp. 1200–1207). doi: 10.1109/ICEMI46757.2019.9101798.

Chen, Y., Dong, H., Lu, J., Sun, X., & Guo, L. (2016). A super-twisting-like algorithm and its application to train operation control with optimal utilization of adhesion force. *IEEE Transactions on Intelligent Transportation Systems*, *17*(11), 3035–3044. doi: 10.1109/TITS.2016.2539361.

Chen, Q., Ge, X., Chen, S., Wang, J., & Wang, K. (2025). Traction optimization of locomotive startup considering axle load transfer. *Journal of Mechanical Science and Technology*, *39*(5), 2443–2453. doi: 10.1007/s12206-025-0405-0.

Diao, L., Zhao, L., Jin, Z., Wang, L., & Sharkh, S. M. (2017). Taking traction control to task: High-adhesion-point tracking based on a disturbance observer in railway vehicles. *IEEE Industrial Electronics Magazine*, *11*(1), 51–62. doi: 10.1109/MIE.2016.2644699.

Georgatzi, V. V., Stamboulis, Y., & Vetsikas, A. (2020). Examining the determinants of CO2 emissions caused by the transport sector: Empirical evidence from 12 European countries. *Economic Analysis and Policy*, *65*, 11–20. doi: 10.1016/j.eap.2019.11.003.

Guo, F., & He, J. (2024). Optimal allocation method of electric/air braking force of high-speed train considering axle load transfer. *High-Speed Railway*, *2*(2), 77–84.

Huang, D., Yang, W., Huang, T., Qin, N., Chen, Y., & Tan, Y. (2021). Iterative learning operation control of high-speed trains with adhesion dynamics. *IEEE Transactions on Control Systems Technology*, *29*(6), 2598–2608. doi: 10.1109/TCST.2021.3049958.

Ishikawa, Y., & Kawamura, A. (1997). Maximum adhesive force control in super high speed train. In *Proceedings of Power Conversion Conference - PCC '97* (Vol. 2, pp. 951–954). doi: 10.1109/PCCON.1997.638382.

Kadowaki, S. ., Ohishi, K. ., Hata, T. ., Iida, N. ., Takagi, M., Sano, T., & Yasukawa, S. (2007). Antislip readhesion control based on speed-sensorless vector control and disturbance observer for electric commuter train–Series 205-5000 of the East Japan railway company. *IEEE Transactions on Industrial Electronics*, *54*(4), 2001–2008. doi: 10.1109/TIE.2007.895135.

Liu, Y., Jiang, T., Zhao, X., Wen, Z., & Jin, X. (2020). Effects of axle load transfer on wheel rolling contact fatigue of high-power AC locomotives with oblique traction rods. *International Journal of Fatigue*, *139*, 105748. doi: 10.1016/j.ijfatigue.2020.105748.

Liu, R., Chen, Z., & Wang, J. (2023). Optimal adhesion control method for railway trains based on reset control sliding mode extremum seeking algorithm. In *2023 7th Asian Conference on Artificial Intelligence Technology (ACAIT)* (pp. 883–888). doi: 10.1109/ACAIT60137.2023.10528638.

Liu, Y., Wu, X., Ma, P., & Yuan, X. (2025). Optimization and validation of traction performance for an eight-axle heavy-haul locomotive during gradient starting. *Scientific Reports*, *15*(1), 45144. doi: 10.1038/s41598-025-33173-6.

Lu, K., Song, Y., & Cai, W. (2014). Robust adaptive re-adhesion control for high speed trains. In *17th International IEEE Conference on Intelligent Transportation Systems (ITSC)* (pp. 1215–1220). doi: 10.1109/ITSC.2014.6957853.

Ma, Y., Ma, W., Li, M., Liu, Q., Luo, S., Wang, Y., & Lei, C. (2025). Research on the structural strength of medium and low speed maglev vehicle levitation frame based on full-scale test bench. *Engineering Failure Analysis*, *180*, 109901. doi: 10.1016/j.engfailanal.2025.109901.

Moaveni, B., Fathabadi, F. R., & Molavi, A. (2020). Supervisory predictive control for wheel slip prevention and tracking of desired speed profile in electric trains. *ISA Transactions*, *101*, 102–115. doi: 10.1016/j.isatra.2020.01.011.

Molavi, A., & Rashidi Fathabadi, F. (2022). Robust model predictive anti-slip controller and speed profile tracking of an electric train based on LMI approach. *International Journal of Dynamics and Control*, *10*(6), 1943–1954. doi: 10.1007/s40435-022-00931-7.

Sadr, S., Khaburi, D. A., & Rodríguez, J. (2016). Predictive slip control for electrical trains. *IEEE Transactions on Industrial Electronics*, *63*(6), 3446–3457. doi: 10.1109/TIE.2016.2543180.

Spiryagin, M., Lee, K. S., & Yoo, H. H. (2008). Control system for maximum use of adhesive forces of a railway vehicle in a tractive mode. *Mechanical Systems and Signal Processing*, *22*(3), 709–720. doi: 10.1016/j.ymssp.2007.09.018.

Uyulan, Ç., & Gokasan, M. (2018). Modeling, simulation and re-adhesion control of an induction motor–based railway electric traction system. *Proceedings of the Institution of Mechanical Engineers - Part I: Journal of Systems and Control Engineering*, *232*(1), 3–11. doi: 10.1177/0959651817732487.

Wen, X., Huang, J., & Zhang, S. (2019). Anti-slip re-adhesion control strategy of electric locomotive based on distributed MPC. In *2019 IEEE 21st International Conference on High Performance Computing and Communications; IEEE 17th International Conference on Smart City; IEEE 5th*

International Conference on Data Science and Systems (HPCC/SmartCity/DSS) (pp. 2708–2713). doi: 10.1109/HPCC/SmartCity/DSS.2019.00380.

Yamashita, M., & Soeda, T. (2015). Anti-slip re-adhesion control method for increasing the tractive force of locomotives through the early detection of wheel slip convergence. In *2015 17th European Conference on Power Electronics and Applications* (pp. 1–10). EPE'15 ECCE-Europe). doi: 10.1109/EPE.2015.7311756.

Yuan, Z., Wu, M., Tian, C., Zhou, J., & Chen, C. (2021). A review on the application of friction models in wheel-rail adhesion calculation. *Urban Rail Transit*, *7*(1), 1–11. doi: 10.1007/s40864-021-00141-y.

Zhao, K., Li, P., Zhang, C., He, J., Li, X., & Liu, J. (2019). Optimal utilization of adhesion force for heavy-haul electric locomotive based on extremum seeking with sliding mode and asymmetric barrier Lyapunov function. *Journal of Advanced Transportation*, *2019*, 1–15. doi: 10.1155/2019/6270515.

Corresponding author
Kan Liu can be contacted at: bjliukan@163.com